doi: 10.82124/CEAS-GNC-2026-072 CEAS-GNC-2026-072

Performance and robustness analysis of INDI flight control laws with $\mathcal{L}_1$ adaptive augmentation

Giorgio Raos Research Fellow, Dipartimento di Scienze e Tecnologie Aerospaziali, Politecnico di Milano, Via La Masa 34, 20156 Milano. giorgio.raos@polimi.it

Giovanni Gozzini Postdoctoral Research Fellow, Dipartimento di Scienze e Tecnologie Aerospaziali, Politecnico di Milano, Via La Masa 34, 20156 Milano. giovanni.gozzini@polimi.it

Davide Invernizzi Associate Professor, Dipartimento di Scienze e Tecnologie Aerospaziali, Politecnico di Milano, Via La Masa 34, 20156 Milano. davide.invernizzi@polimi.it

Keywords: Incremental Nonlinear Dynamic Inversion; Adaptive Control; Aircraft Flight Control Systems; Robustness analysis

ABSTRACT

This work presents the analysis of performance and robustness properties of different INDI architectures, together with the evaluation of the effectiveness of an $\mathcal{L}_1$ Piecewise Constant (PwC) adaptive augmentation, designed to compensate for perturbations in the dynamics. Using as application scenario the nonlinear longitudinal dynamics of a tail-controlled airframe, an INDI pitch rate control loop is designed within the cascade of a climb angle autopilot. The differences between model-based and sensor-based INDI control laws are highlighted both in the time-domain and in the frequency-domain, and a sensitivity study is performed with respect to the tuning parameters of the adaptive augmentation. The results highlight performance and robustness tradeoffs in the design of the adaptive controller when considering different baseline INDI architectures, offering valuable insights on the tuning of these innovative control systems.

1 Introduction

To achieve stability, most modern fixed-wing aircraft adopt a Flight Control System (FCS) which uses gain-scheduling (GS). In this approach, the varying system dynamics and nonlinearities are taken into account by switching the controller parameters, based on scheduling variables. Although there exist techniques that partially automate the scheduling process [1], a significant effort may still be required, and the full capabilities of the aircraft may not be exploited. To address this issue, in the last decade Incremental Nonlinear Dynamic Inversion (INDI) has become a popular solution in the aerospace sector [2]. This control design method, introduced by Smith in 1998 [3], can be applied to the control of fixed-wing aircraft to achieve a decoupled response across the full envelope, and to embed the desired flying qualities inside the controller [4]. Moreover, the use of an accurate angular acceleration sensor and a high controller update rate can render the performance minimally affected by aerodynamic model mismatches [5]. However, in real-world applications, the difficult installation of angular accelerometers poses an important challenge to the control designer [6]. Filtering and differentiation of gyroscopic data [7] is a popular alternative although it introduces a dynamic perturbation into the INDI loop [8]. For this reason, reinstating the model information in a hybrid [9, 10] or fully model-based [11] architecture

can sometimes prove to be advantageous [12]. The choice of the architecture ultimately becomes a trade-off, as the model-based approach results in a greater dependence of the performance on the model accuracy, which is typical of standard NDI controllers [13]. To improve performance under perturbations in the dynamics, the use of adaptive controllers has been investigated in literature. Among the possible architectures, $\mathcal{L}_1$ control [14] has gained popularity in recent years, as it was shown to have a reduced impact on the robustness of the system [15] compared to more traditional model reference adaptive controllers [16]. Augmenting baseline NDI control laws, the $\mathcal{L}_1$ adaptive controller was designed for the compensation of residual inversion errors in [17–20], with an architecture in which the adaptive control contribution is summed to the pseudo control input, similarly to previous works [21, 22]. In the context of aircraft INDI control laws, an augmentation of the inner linearization loop was proposed in [23], where the authors showed that with a model-based baseline INDI controller the adaptive augmentation provides significant improvements of the performance in uncertain scenarios. In [24] a similar adaptive structure was used in augmentation to a sensor-based INDI controller, observing minor improvements in performance. Therefore, the benefit of augmenting INDI controllers with traditional disturbance-compensating adaptive controllers remains to be clarified.
The objective of this work is to investigate the performance and robustness properties of different INDI architectures and evaluate the effectiveness of an $\mathcal{L}_1$ Piecewise Constant (PwC) adaptive augmentation to a nominal design of a baseline INDI controller, from both methodological and numerical perspectives. The focus is placed on the analysis of the possible stability degradations which occur when the adaptive augmentation is plugged in, despite the expected performance improvement.
The rest of the paper is organized as follows: Section 2 presents the general formulation of INDI control laws. Section 3 introduces the $\mathcal{L}_1$ PwC adaptive plant augmentation design, and provides theoretical insights into the tuning of this component. In Section 4 the studied application scenario corresponding to the design of a longitudinal autopilot is presented, while the results obtained through the frequency-domain analysis is presented in Section 5. Section 6 draws the final conclusions on the work.

2 Incremental Nonlinear Dynamic Inversion

This section serves as an introduction to the main ideas in Incremental Nonlinear Dynamic Inversion (INDI). In Section 2.1 the control law for a general nonlinear system is derived, while in section 2.2 some variations on the control architecture are discussed, together with the tuning and implementation of INDI controllers in flight control systems for fixed-wing aircraft.

2.1 General INDI theory

The following nonlinear plant dynamics is considered:

$$\begin{cases} \dot{x} = f(x,u) & \text{(1a)} \\ y = h(x), & \text{(1b)} \end{cases}$$

where $x \in \mathbb{R}^n$ is the state vector, $u \in \mathbb{R}^m$ is the input vector, $y \in \mathbb{R}^m$ is the output vector, with $f : \mathbb{R}^n \times \mathbb{R}^m \to \mathbb{R}^n$ and $h : \mathbb{R}^n \to \mathbb{R}^m$ being nonlinear functions that are differentiable with respect to their arguments. Considering available state and input feedback, the control objective is to track a piecewise continuous and differentiable signal $r(t) : \mathbb{R} \to \mathbb{R}^m$ that represents the desired value of the output vector.
For the output dynamics:

$$\dot{y} = \frac{\partial h(x)}{\partial x}\dot{x} = \frac{\partial h(x)}{\partial x} f(x,u), \tag{2}$$

the Taylor expansion of (2) around $x_0 := x(t - \Delta t)$, $u_0 := u(t - \Delta t)$ is considered [6], where Δt is the controller sampling rate. Neglecting the terms of order higher than one results in:

$$\dot{y} = \dot{y}_0 + F(x_0, u_0)\Delta x + G(x_0, u_0)\Delta u, \tag{3}$$

where $\Delta x := x - x_0$ and $\Delta u := u - u_0$ are respectively the state vector and input vector increments, and

$$F(x_0, u_0) := \left.\frac{\partial h(x)}{\partial x}\right|_{x_0} \left.\frac{\partial f(x,u)}{\partial x}\right|_{(x_0,u_0)} \qquad G(x_0, u_0) := \left.\frac{\partial h(x)}{\partial x}\right|_{x_0} \left.\frac{\partial f(x,u)}{\partial u}\right|_{(x_0,u_0)}. \tag{4}$$

With a timescale separation argument, the term involving the state increment Δx in equation (3) can be neglected [2]. This assumption is reasonable given a sufficiently high sampling rate of the controller and actuator bandwidth. The simplified incremental dynamics then becomes

$$\dot{y} \approx \dot{y}_0 + G(x_0, u_0)\Delta u, \tag{5}$$

where the input map $G(x_0, u_0) : \mathbb{R}^n \times \mathbb{R}^m \to \mathbb{R}^{m\times m}$ is assumed to yield a non-singular matrix for all admissible values of x and u. To obtain the control law, the fast dynamics of the actuation devices is neglected, so that $\Delta u \approx u_{\text{cmd}} - u_0 =: \Delta u_{\text{cmd}}$, and the pseudo control input $\nu(t) \in \mathbb{R}^m$ is then defined as

$$\nu = \dot{y}_0 + G(x_0, u_0)\Delta u_{\text{cmd}}. \tag{6}$$

By inverting equation (6), the incremental command is computed as:

$$\Delta u_{\text{cmd}} = G(x_0, u_0)^{-1}\,(\nu - \dot{y}_0), \tag{7}$$

while the total command for the input vector can be retrieved as $u_{\text{cmd}} = \Delta u_{\text{cmd}} + u_0$. Under the aforementioned assumptions, we can substitute control law (7) in equation (5) to get

$$\dot{y} = \nu, \tag{8}$$

meaning that ν can be used as a design variable that represents the desired value for the time derivatives of the output vector components, whose dynamics are now decoupled and given by an integrator. The controller computing the pseudo-control input ν can be designed with simple linear methods that achieve closed-loop stability while making the tracking error $e = r - y$ asymptotically vanish.

2.2 Variations and implementation remarks on the INDI architecture

In real-world applications, the model is not known exactly. The control designer typically works with the best available estimate of the input map, which we denote as $\hat{G}(x, u)$, and could come from some online estimation process, or from some offline identification campaign. A more accurate $\hat{G}$ yields a linearized output dynamics that more closely matches (8). Throughout the paper, we will make use of an input map computed through an On-Board Model (OBM), as

$$\hat{G}(x_0, u_0) := \left.\frac{\partial h(x)}{\partial x}\right|_{x_0} \left.\frac{\partial \hat{f}(x,u)}{\partial u}\right|_{(x_0,u_0)}. \tag{9}$$

The second element of control law (7) affected by uncertainty is the output derivative $\dot{y}_0$. If a complete model of the system $\hat{f}(x, u)$ is available and stored in the OBM, then a fully Model-Based (MB) INDI

architecture can be employed, where

$$\begin{aligned} \Delta u_{\text{cmd,mb}} &= \hat{G}(x_0, u_0)^{-1}(\nu - \dot{y}_{0,\text{mb}}), \quad u_{\text{cmd}} = \Delta u_{\text{cmd,mb}} + u_0 \\ \dot{y}_{0,\text{mb}} &= \frac{\partial h(x)}{\partial x} \hat{f}(x,u)\Big|_{x_0,u_0} \end{aligned} \tag{10}$$

Similar to standard NDI, a complete model of the system is required [9], which could raise the development costs. Moreover, the closed-loop system performance is also affected by model mismatches. In the case of flight control systems, the biggest source of uncertainty usually resides in the aerodynamic model. An advantage of the model-based architecture is that with a unique OBM the full system dynamics are available, and the choice of the output vector can change easily as the sensing unit is not tied to the choice of the output vector.

A popular alternative to the model-based INDI is sensor-based (SB) INDI, in which the online computation of the output derivative is replaced via direct measurements. In the design of flight control systems for fixed-wing aircraft, the output vector typically represents the aircraft body rates. Given that sensors for direct measurement of angular acceleration are rare [6], a more common solution is to process gyroscopic data in a suitable way. To prevent high levels of noise from entering the feedback path, a simple filter can be used so that

$$\dot{y}_{0,\text{sb}}(s) = H_{\text{f}}(s)\dot{y}_0(s), \tag{11}$$

where s is the Laplace variable and $H_f(s)$ is usually a first or second order low-pass filter. An ideal sensor (*i.e.* a filter $H_f(s)$ with high bandwidth) would pick up any plant mismatch, which is then compensated incrementally in the inner linearization loop. For this reason, it shown in [5] that sensor-based INDI control laws are particular insensitive to slow-varying disturbances that perturb the output dynamics.

As the Taylor expansion performed in equation (3) should contain time-coherent measurements, it was observed in [7] that replicating the low-pass filter in the actuator feedback path increases robustness. The synchronized SB INDI control law is therefore given by:

$$\begin{aligned} \Delta u_{\text{cmd,sb}} &= \hat{G}(x_0, u_{0,\text{f}})^{-1}(\nu - \dot{y}_{0,\text{sb}}), \quad u_{\text{cmd}} = \Delta u_{\text{cmd,sb}} + u_{0,\text{f}}, \\ u_{0,\text{f}}(s) &= H_{\text{f}}(s)u_0. \end{aligned} \tag{12}$$

Lastly, the design of the pseudo control ν is considered. While the inner state-feedback loop is the backbone of the architecture, adopting $\nu = \dot{r}$ is not acceptable in a practical implementation, as it corresponds to marginally stable output dynamics. An outer loop with a linear controller that provides stability while specifying a desired response is commonly adopted. For this reason (I)NDI control laws have become popular in the aerospace industry, as their modular structure [8], [4] reduces the effort required in the transition from design requirements to controller tuning. Nevertheless, it could be advantageous to augment the control structure with an adaptive controller explicitly tasked with fast online compensation of unknown perturbations in the dynamics, as done in recent literature [24], [23] using an architecture which will be presented in the next section.

3 $\mathcal{L}_1$ adaptive augmentation of INDI controllers

In this section we present the $\mathcal{L}_1$ adaptive augmentation developed to recover the nominal closed-loop response of the INDI controller discussed in the previous section. In Section 3.1 the problem setup is presented, In Section 3.2 we derive the $\mathcal{L}_1$ PwC adaptive controller in a plant augmentation scheme, and finally in Section 3.3 we cover some remarks on the tuning and implementation of the considered adaptive controller.

3.1 Uncertain incremental output dynamics

Uncertainty in the input map and in the estimation of the output derivative will now be explicitly addressed. Equation (5) can be rewritten neglecting the fast actuator dynamics as

$$\dot{y} = \dot{y}_{0,\mathrm{mb/sb}} + \tilde{\dot{y}}_0 + \hat{G}\Lambda\Delta u_{\mathrm{tot}}, \tag{13}$$

where $\tilde{\dot{y}}_0 \coloneqq \dot{y}_0 - \dot{y}_{0,\mathrm{mb/sb}}$, is the output derivative estimation error, $\Lambda \in \mathbb{R}^{m\times m}$ is a positive definite matrix such that $G = \hat{G}\Lambda$, modeling an uncertain multiplicative control effectiveness. Following an augmentation approach, the input increment is split as

$$\Delta u_{\mathrm{tot}} = \Delta u_{\mathrm{bl}} + \Delta u_{\mathrm{ad}}, \tag{14}$$

where Δu_{bl} and Δu_{ad} are computed by the baseline INDI and the adaptive controller respectively. For an *a priori* estimate Λ_0 of the control effectiveness, equation (13) can be rewritten as

$$\begin{aligned}\dot{y} &= \dot{y}_{0,\mathrm{mb/sb}} + \hat{G}[\Lambda_0\Delta u_{\mathrm{tot}} + \underbrace{(\Lambda - \Lambda_0)\Delta u_{\mathrm{tot}} + \hat{G}^{-1}\tilde{\dot{y}}_0}_{\sigma}] \\ &= \dot{y}_{0,\mathrm{mb/sb}} + \hat{G}(\Lambda_0\,\Delta u_{\mathrm{tot}} + \sigma),\end{aligned} \tag{15}$$

where the uncertainties have been lumped in $\sigma \in \mathbb{R}^m$, representing a disturbance matched in the control channel. This setup is suitable for the design of an $\mathcal{L}_1$ Piecewise Constant (PwC) adaptive controller, as presented in the next section.

3.2 $\mathcal{L}_1$ Piecewise Constant adaptive architecture

Adaptive controllers adjust their control parameters in real time through an automated process of adaptation based on measurements, with the objective of compensating for system uncertainties and variations. Differently from standard model reference adaptive control, in $\mathcal{L}_1$ adaptive control theory [14] a low-pass filter in the control law is used to prevent high-frequency oscillations from entering the input channel, which is fundamental in safety-critical systems [25].

In this architecture, the uncertainty estimate update law is driven by the error between the state of a predictor and the measured output. The adaptive control law then employs this estimate to compensate for the uncertainty in the system dynamics, aiming to recover the nominal response. Each component of the $\mathcal{L}_1$ PwC adaptive controller is now explained in more detail.

The predictor replicates the dynamics (15), and is defined by:

$$\dot{\hat{y}} = \dot{y}_{0,\mathrm{sb/mb}} + \hat{G}(\Lambda_0\Delta u_{\mathrm{tot}} + \hat{\sigma}) - L(\hat{y} - y), \quad \hat{y}(t_0) = \hat{y}_0 \tag{16}$$

where $\hat{y} \in \mathbb{R}^m$ is the state of the predictor and $L \in \mathbb{R}^{m\times m}$ is a positive definite gain matrix. The update law for the uncertainty estimate $\hat{\sigma} \in \mathbb{R}^m$ is based on the prediction error $\tilde{y} \coloneqq \hat{y} - y$, whose dynamics are given by:

$$\dot{\tilde{y}} = -L\tilde{y} + \hat{G}(\hat{\sigma} - \sigma). \tag{17}$$

The update law for $\hat{\sigma}$ is piecewise constant, and given by [26]:

$$\hat{\sigma}(t) = K_{\mathcal{L}_1}(T_s)\tilde{y}(iT_s), \quad \forall t \in [iT_s, (i+1)T_s), \tag{18}$$

where $i \in \mathbb{N}_0$ and

$$K_{\mathcal{L}_1}(T_s) \coloneqq -\hat{G}^{-1}(I_m - e^{-LT_s})^{-1}Le^{-LT_s} \tag{19}$$

is a gain that depends on L and on the controller sampling rate T_s, with the latter generally made as small as the available computational power allows. As mentioned earlier, the baseline controller is designed to meet the control objective under nominal conditions, and the adaptive input should simply compensate for the matched disturbance in the plant. This leads to the following adaptive control law:

$$\Delta u_{\text{ad}}(s) = -\Lambda_0^{-1} C(s)\hat{\sigma}(s), \tag{20}$$

where $\hat{\sigma}(s)$ denotes the Laplace transform of $\hat{\sigma}(t)$, while $C(s) \in \mathbb{R}^{m\times m}$ is a diagonal matrix composed of m stable low-pass filters:

$$C(s) = \text{diag}(C_1(s), \ldots, C_m(s)). \tag{21}$$

In this way, one avoids introducing high frequency oscillations in the control channel. The filter bandwidth is maximized subject to the available bandwidth, and such that the $\mathcal{L}_1$-norm condition [14]

$$||G_{\mathcal{L}_1}(s)||_{\mathcal{L}_1} < k \tag{22}$$

is satisfied, where k is a small positive value, and $G_{\mathcal{L}_1}(s) \in \mathbb{R}^{m\times m}$ is a transfer function defined as:

$$G_{\mathcal{L}_1}(s) \coloneqq (sI_m + L)^{-1}\hat{G}(I_m - C(s)). \tag{23}$$

3.3 Further remarks on the $\mathcal{L}_1$ PwC architecture

Fig. 1 shows the closed loop prediction error dynamics, together with the resulting adaptive control law contribution. This block diagram is obtained by combining equations (17) and (18), for a small sampling rate $T_s \to 0$. As expected, the low-pass filter $C(s)$ which is part of the control law does not affect the error dynamics, because it enters identically in the plant and in the predictor. The gain $L > 0$

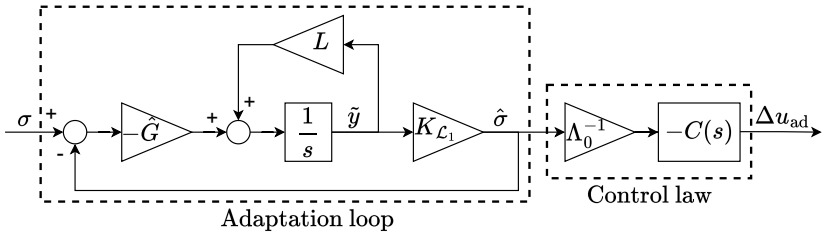

Fig. 1 The decoupling between the fast adaptation loop and the filtered control in the $\mathcal{L}_1$ controller.

is necessary to make the origin of the prediction error dynamics an asymptotically stable equilibrium, however, since the source of this adaptation is the mismatch between plant and predictor, a large L which damps out the prediction error too fast prevents accurate disturbance estimation.

We can more thoroughly investigate the estimation performance by computing the transfer function from the unknown lumped uncertainty σ to its estimate $\hat{\sigma}$, denoted as $F_\sigma(s)$. Considering for simplicity the SISO case with $m = 1$, combining the block diagram in Fig. 1 with the definition of $K_{\mathcal{L}_1}$ of equation (19) we get after some mathematical passages

$$F_\sigma(s) = -K_{\mathcal{L}_1}\left(s - (-L + \hat{G}\,K_{\mathcal{L}_1})\right)^{-1}\hat{G} = \frac{\left(1 - e^{-LT_s}\right)^{-1} L\, e^{-LT_s}}{s + L + \left(1 - e^{-LT_s}\right)^{-1} L\, e^{-LT_s}} = \frac{e^{-LT_s}}{1 \;+\; s\left(\frac{1-e^{-LT_s}}{L}\right)}. \tag{24}$$

From equation (24) it follows that $F_\sigma(0) = e^{-LT_s}$, so that $\lim_{t\to\infty}[\hat{\sigma}(t) - \sigma(t)] \xrightarrow{L\to 0} 0$, *i.e.*, the steady-state estimation error can be rendered arbitrary small by reducing the stabilizing gain L. However, a small L also reduces the stability of the prediction dynamics.

For the complete closed-loop, in [27] it is observed that the $\mathcal{L}_1$ adaptive controller increases the gain-crossover frequency, therefore reducing the corresponding phase margins. Considering an INDI baseline, in [23] the augmentation of a model-based architecture showed to greatly improve performance, while in [24] the same adaptive augmentation applied to a sensor-based INDI provided only minor improvement in performance over the standalone baseline controller. It should be noted that in both works only time-domain analyses were performed. In the following section, a model of the longitudinal dynamics of a fixed-wing aircraft is presented, and frequency-domain analyses are used to complement findings obtained from the time-domain behavior of the closed-loop systems with an without the adaptive augmentation.

4 Application scenario: climb angle autopilot

A climb angle autopilot for a high-performance fixed-wing aircraft is considered. A cascade structure makes sure that the variables controlled in each loop have faster dynamics than the ones in the outer loops, following the typical timescale separation of dynamics and kinematics of rigid bodies. For the inner loop controller both the MB and SB INDI controllers are considered, augmented with the same $\mathcal{L}_1$ PwC adaptive controller.

4.1 Longitudinal airframe model

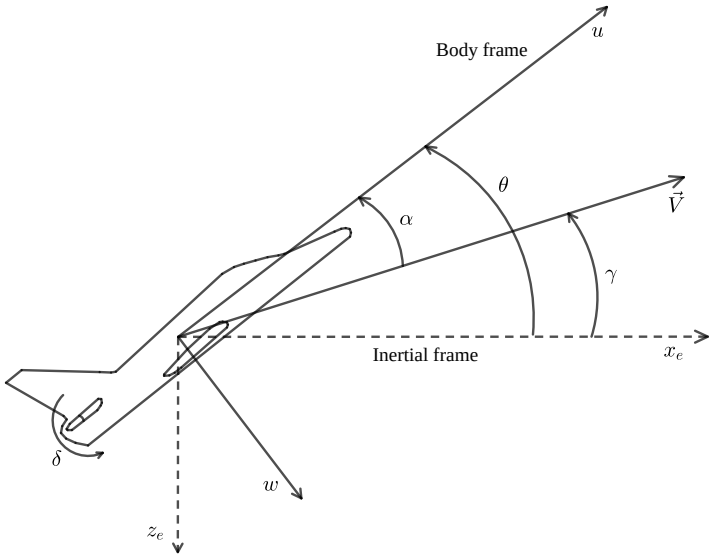

Fig. 2 Longitudinal motion of the airframe in inertial and body frames.

The motion inside the plane of symmetry of the aircraft is described in both the body and inertial frames, and is depicted in Fig. 2. The dynamics is represented by the Newton-Euler equations for the longitudinal and vertical body velocity components, respectively U and w, and for the pitch rate q. The kinematics of the pitch angle θ and the vertical component of the position vector with respect to the fixed-earth frame z_e are also included. The complete airframe is therefore represented through the

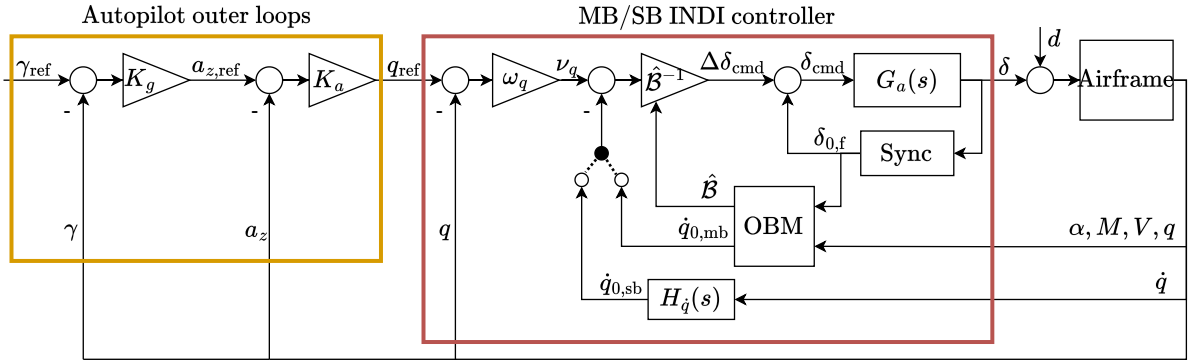

Fig. 3 Overview of the structure of the longitudinal autopilot with the INDI controller.

following system of differential equations:

$$\begin{cases} m\dot{U} = \mathcal{X} + T + m(qw - g\sin\theta) & \text{(25a)} \\ m\dot{w} = \mathcal{Z}_\alpha + \mathcal{Z}_\delta + m(g\cos\theta - qU) & \text{(25b)} \\ J\dot{q} = \mathcal{M}_{\alpha,q} + \mathcal{M}_\delta, & \text{(25c)} \\ \dot{\theta} = q & \text{(25d)} \\ \dot{z}_{\text{e}} = w\cos\theta - U\sin\theta, & \text{(25e)} \end{cases}$$

where $m, J > 0$ are the mass and inertia matrix respectively, g is the gravitational acceleration, $\mathcal{X}$ models a constant drag, $\mathcal{Z}_\alpha$, $\mathcal{M}_{\alpha,q}$ represent nonlinear aerodynamic forces and moments depending on the angle of attack α, with $\mathcal{M}_{\alpha,q}$ including a damping-in-pitch term, $\mathcal{Z}_\delta$ and $\mathcal{M}_\delta$ are the aerodynamic vertical force and moment that depend on the elevator deflection, and T is the total thrust aligned with the first body axis, which is held constant during simulations to simplify the control structure.

The model of the aerodynamic moment is described by the following equations [28]:

$$\begin{aligned} \mathcal{M}_{\alpha,q} &= \frac{1}{2}\rho V^2 S_{\text{ref}} d_{\text{ref}} \left[C_{\mathcal{M}/q} q + C_{\mathcal{M},\alpha}(\alpha, V, M) \right], \\ \mathcal{M}_\delta &= \frac{1}{2}\rho V^2 S_{\text{ref}} d_{\text{ref}} C_{\mathcal{M}/\delta}\delta \end{aligned} \tag{26}$$

where ρ is the atmospheric density, $V = \sqrt{U^2 + w^2}$ is the airspeed, S_{ref} and d_{ref} are the reference surface and length, $C_{\mathcal{M}/q}$ is the damping-in-pitch derivative, and $C_{\mathcal{M},\alpha}$ is a nonlinear function modeling compressibility effects depending on the Mach number M, and $C_{\mathcal{M}/\delta}$ is the control derivative. For the sake of conciseness, the aerodynamic model for the two force components is not expanded as it is not relevant for the control design problem, and the reader is referred to [29] for a more detailed description.

The structure of the climb angle autopilot is shown in Fig. 3. An external climb angle reference signal γ_{ref} is used to compute the corresponding body vertical acceleration command $a_{z,\text{ref}}$ through a proportional controller $a_{z,\text{ref}} = K_{\text{g}}(\gamma_{\text{ref}} - \gamma)$. The middle loop controls the vertical acceleration $a_z = \dot{w}$ by commanding a pitch rate reference signal $q_{\text{ref}} = K_{\text{a}}(a_{z,\text{ref}} - a_z)$. The inner loop is closed around the pitch rate q of the aircraft, and uses the elevator deflection δ. Its baseline structure consists of an INDI controller, which will be repeated in its model-based and sensor-based architectures, as they were presented in Section 2. The structure of the autopilot that was described so far is shown in Fig. 3. The pitch rate dynamics will then be augmented by an $\mathcal{L}_1$ PwC adaptive controller, which follows the derivation presented in Section 3.

4.2 Baseline model-based and sensor-based INDI design

The controlled output of the INDI controller is the pitch rate q of the airframe, whose dynamics are obtained via substitution of the aerodynamic model (26) in equation (25d):

$$\dot{q} = \frac{1}{J} q_\infty S_{\text{ref}} d_{\text{ref}} \left(C_{\mathcal{M}/q} q + C_{\mathcal{M},\alpha}(\alpha, V, M) + C_{\mathcal{M}/\delta} \delta \right), \tag{27}$$

where $q_\infty = \frac{1}{2}\rho V^2$ is the dynamic pressure. The pseudo control input for both the model-based and sensor-based architectures is computed through a proportional controller, so that the desired closed-loop pitch dynamics corresponds to a first order filter $\dot{q} = \nu_q = \omega_q(q_{ref} - q)$, with $\omega_q > 0$.

4.2.1 Model-based INDI design

The model-based INDI architecture is summarized by the following equations:

$$\begin{gathered} \Delta\delta_{\text{cmd,mb}} = \hat{\mathcal{B}}^{-1}(\nu_q - \dot{q}_{0,\text{mb}}), \quad \delta_{\text{cmd}} = \Delta\delta_{\text{cmd,mb}} + \delta_0, \\ \dot{q}_{0,\text{mb}} = \frac{1}{J} q_{\infty,0} S_{\text{ref}} d_{\text{ref}} \left(C_{\hat{\mathcal{M}}/q} q_0 + C_{\hat{\mathcal{M}},\alpha}(\alpha_0, V_0, M_0) + C_{\hat{\mathcal{M}}/\delta} \delta_0 \right), \quad \hat{\mathcal{B}} = \frac{1}{J} q_{\infty,0} S_{\text{ref}} d_{\text{ref}} C_{\hat{\mathcal{M}}/\delta}, \end{gathered} \tag{28}$$

where the subscript 0 denotes measurements at the previous time step, while $C_{\hat{\mathcal{M}}/q}$, $C_{\hat{\mathcal{M}},\alpha}$ and $C_{\hat{\mathcal{M}}/\delta}$ are part of the aerodynamic model stored inside the OBM, which in a nominal scenario matches the true model. Note that since the dynamics (27) is input-affine, the computation of the input map $\hat{\mathcal{B}}$ is not the result of a linear approximation.

4.2.2 Sensor-based INDI design

For the sensor-based INDI architecture, a measurement of the current pitch acceleration is required, and a first-order filter $H_{\dot{q}}$ is used. To address the synchronization of measurements, the same filter is placed in the elevator position feedback path (Sync block in Fig. 3). The sensor-based INDI control law is summarized by the following equations:

$$\begin{gathered} \Delta\delta_{\text{cmd,sb}} = \hat{\mathcal{B}}^{-1}(\nu_q - \dot{q}_{0,\text{sb}}), \quad \delta_{\text{cmd}} = \Delta\delta_{\text{cmd,sb}} + \delta_{0,\text{f}}, \\ \dot{q}_{0,\text{sb}}(s) = H_{\dot{q}}(s)\dot{q}_0(s), \quad \delta_{0,\text{f}}(s) = H_{\dot{q}}(s)\delta_0(s), \quad H_{\dot{q}} = \frac{\omega_{\dot{q}}}{s + \omega_{\dot{q}}}, \end{gathered} \tag{29}$$

where $\omega_{\dot{q}} > 0$ is the bandwidth of the low-pass filter, which should have sufficient frequency separation with respect to the rigid body dynamics [8]. Note that the computation of $\hat{\mathcal{B}}$ is unchanged with respect to the model-based INDI control law.

4.3 Inner loop $\mathcal{L}_1$ adaptive augmentation

In uncertain scenario, we consider the open-loop pitch rate dynamics to be affected by a disturbance σ matched inside the control channel, coming from estimation errors in $\dot{q}_0$ and $\mathcal{B}$ and from exogenous disturbances, such as wind gusts. In the incremental representation (compare with (13)) we get

$$\dot{q} = \dot{q}_{0,\text{mb/sb}} + \hat{\mathcal{B}}(\lambda_0 \Delta\delta_{\text{tot}} + \sigma), \quad \Delta\delta_{\text{tot}} = \Delta\delta_{\text{bl}} + \Delta\delta_{\text{ad}}, \tag{30}$$

where without losing generality it can be assumed that the *a priori* estimate of the unknown control effectiveness is $\lambda_0 = 1$. The predictor is then given by:

$$\dot{\hat{q}} = \dot{q}_{0,\text{mb/sb}} + \hat{\mathcal{B}}(\lambda_0 \Delta\delta_{\text{tot}} + \hat{\sigma}) - L(\hat{q} - q). \tag{31}$$

The update law for $\hat{\sigma}$ is derived from the prediction error $\tilde{q} := \hat{q} - q$ sampled at the rate of the controller T_s, and is given by:

$$\hat{\sigma}(t) = K_{\mathcal{L}_1}(T_s)\tilde{q}(iT_s), \quad \forall t \in [iT_s, (i+1)T_s), \tag{32}$$

with

$$K_{\mathcal{L}_1}(T_s) = -\hat{\mathcal{B}}^{-1}(1 - e^{-LT_s})^{-1}Le^{-LT_s}. \tag{33}$$

For the $\mathcal{L}_1$ adaptive control law, a simple first-order filter design is chosen, so that in the Laplace domain

$$\Delta\delta_{\text{ad}}(s) = -\lambda_0^{-1}C(s)\hat{\sigma}(s), \quad C(s) = \frac{\omega_{\text{f}}}{s + \omega_{\text{f}}}. \tag{34}$$

with ω_{f} being the frequency range over which the uncertainty must be compensated for. Note that in this formulation the actuator dynamics is neglected, as it is sufficiently fast and therefore not included in the predictor. However, this has repercussions on the response of the system, and a certain degree of intrusiveness of the adaptive controller is expected during maneuvers, where a mismatch between the predictor and the plant is inevitable. The interconnection of the $\mathcal{L}_1$ PwC adaptive controller with the rest of the control system is shown in Fig. 4.

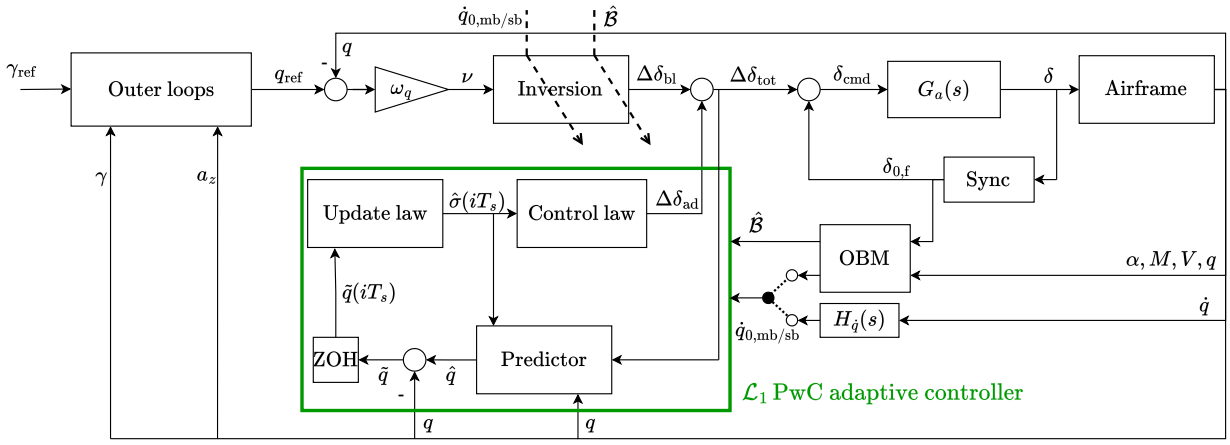

Fig. 4 Interconnection of the $\mathcal{L}_1$ PwC adaptive controller with the baseline INDI controller.

4.4 Nonlinear time-domain simulations

The control system and the longitudinal airframe dynamics is implemented in MATLAB/Simulink®, together with an actuator modeled as a second order filter $G_a(s) = \frac{\omega_n^2}{s^2+2\zeta\omega_n s+\omega_n^2}$, with $\zeta = 0.7$ and $\omega_{\text{n}} = 150\,\text{rad/s}$. The sampling period of the baseline INDI controller is $dt = 0.01$ s.

The two proportional outer loops controllers K_{g} and K_{a} are tuned using the MATLAB® function `systune`, which uses non-smooth optimization algorithms to perform a structured synthesis based on multiple performance specifications, which are explained in more detail in [29]. The same pseudo controller was tuned for both architectures of the INDI controller, using as benchmark the gain-scheduled autopilot designed on the same airframe model in [1]. The bandwidth of the filter in the $\mathcal{L}_1$ adaptive controller was selected conservatively with respect to the actuator speed, and the stabilizing gain L was obtained by using the equation for the steady state estimation derived under equation (24), desiring a value of $F_\sigma(s = 0) = 0.99$. The values for the tuned parameters are shown in Tab. 1

Firstly, a simulation featuring a disturbance at the plant input (as shown in Fig. 3) $d(t) = 8\,\text{step}(t - 10)$ deg is considered. To initialize simulations, the open-loop aircraft is trimmed at $V = 700\,\text{m/s}$, $h = 3000\,\text{m}$ using the MATLAB ® function `findop`. Fig. 5 shows the response obtained while commanding an angle of climb γ_{ref} that makes the system cross its operational envelope. The standalone model-based INDI does not achieve satisfactory performance, as expected given that it does not feature an integral

Table 1 The tuned parameters of the control system.

K_g	-1324
K_a	-0.0093
ω_q	12 rad/s
$\omega_{\dot{q}}$	80 rad/s
T_s	0.01 s
ω_f	50 rad/s
L	1

contribution. For both baseline INDI architectures the adaptive controller shows to compensate the disturbance similarly, although the sensor-based INDI controller as a standalone presents a sufficiently fast compensation of the disturbance. To focus on the inner loop controlling the pitch rate of the aircraft,

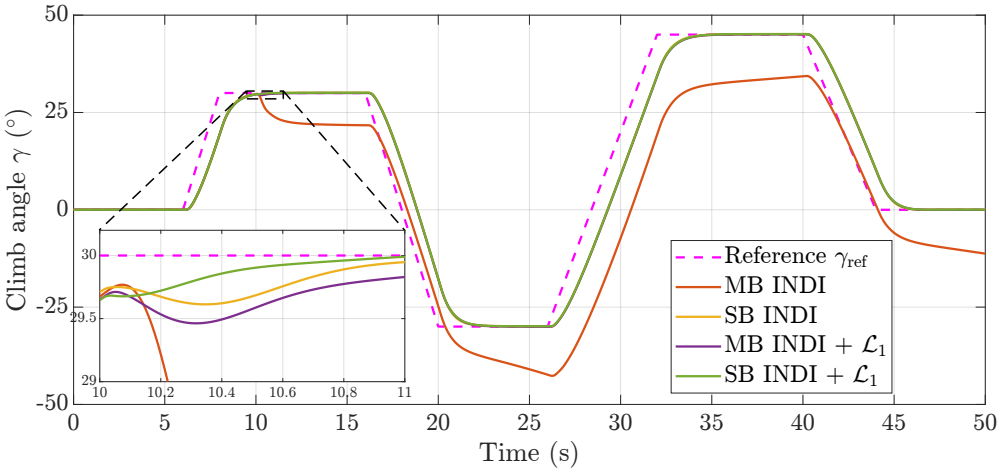

Fig. 5 Climb angle response with step disturbance, for sensor-based and model-based architectures with and without the $\mathcal{L}_1$ adaptive augmentation.

simulations with the outer loops disengaged are also performed. A doublet signal for q_{ref} is provided to the INDI controller, and the results with and without the $\mathcal{L}_1$ adaptive augmentation are shown in Fig. 6. It is possible to see that both the model-based and sensor-based do not respond in the ideal way, but the adaptive augmentation recovers the tuned nominal closed-loop response. It can also be seen that augmentation of the sensor-based INDI provides the fastest compensation, although it presents an overshoot in the pitch rate response. In the next section, these properties of the responses are connected to the performance and stability of the system using frequency-domain insights.

5 Frequency-domain performance and robustness analysis

This section presents the main results of the work, where the effectiveness of the $\mathcal{L}_1$ adaptive augmentation is evaluated. In section 5.1 the process of obtaining the linear approximation of the closed loop is explained. Then, in Section 5.2 the performance and robustness properties of the closed-loop system are derived in the frequency-domain, considering multiple designs for the autopilot in terms of INDI architecture and $\mathcal{L}_1$ controller tuning.

5.1 Trim and linearization methodology

To analyze the stability of the system in the neighborhood of a given equilibrium point, a linearization of the bare airframe around a trim solution is considered. Then, based on the linear approximation of the

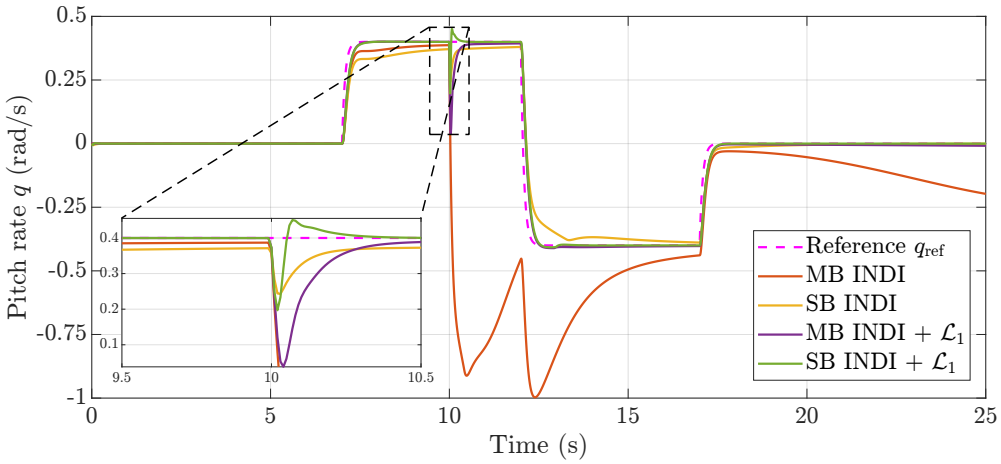

Fig. 6 Pitch rate response with step disturbance, for sensor-based and model-based architectures with and without $\mathcal{L}_1$ adaptive augmentation

plant dynamics, a linear Incremental Dynamic Inversion (IDI) controller is constructed, which behaves similarly to the nonlinear counterpart when the system remains close to the equilibrium point. The rest of the autopilot components, including the two outer loop proportional controllers and the $\mathcal{L}_1$ PwC adaptive controller, do not need linearization as already composed by LTI components.

5.1.1 Airframe Linearization

For a given value of V and h, the linear representation of the airframe dynamics is obtained using the MATLAB® function `linearize`. The airframe dynamics is represented by:

$$\begin{cases} \dot{x}_{\text{ba}} = A_{\text{ba}} x + B_{\text{ba}} \delta \\ y_{\text{m}} = C_{\text{ba}} x + D_{\text{ba}} \delta \end{cases} \tag{35}$$

where $x_{\text{ba}} = [U, w, q, \theta, z_e]^\top$ is the state vector, and $y_{\text{m}} = [x_{\text{ba}}^\top, \dot{q}, \gamma, a_z]^\top$ is a linear combination of the state and of the input, which represents the response of the system. The IDI controller then focuses on the linearized pitch rate dynamics given by

$$\dot{q} = C_{\dot{q}} x_{\text{ba}} + D_{\dot{q}} \delta, \tag{36}$$

where $C_{\dot{q}} \in R^{1\times 5}$ and $D_{\dot{q}} \in R$ are the coefficients of the pitch acceleration output equation. Leveraging a Taylor expansion, the approximate incremental output dynamics is given by:

$$\dot{q} = \dot{q}_0 + D_{\dot{q}} \Delta\delta. \tag{37}$$

Notice that for the linear system $D_{\dot{q}}$ represents the (constant) input map, directly extracted from the linearization of the system.

5.1.2 Controller linearization

For the model-based IDI the pitch acceleration estimation module is a static computation which replicates the output equation for $\dot{q}$. Defining the input vector to the linear OBM as $z = [\delta, x_{\text{ba}}^\top]^\top$, then $\dot{q}_{0,\text{mb}} = D_{\text{obm}} z_0$, with $D_{\text{obm}} = [D_{\dot{q}}, C_{\text{q}}]$. The IDI control laws for the two architectures follow naturally, and are given by

$$\begin{gathered} \Delta\delta_{\text{cmd,mb}} = D_{\dot{q}}^{-1}(\nu_q - \dot{q}_{0,\text{mb}}), \quad \delta_{\text{cmd}} = \Delta\delta_{\text{cmd,mb}} + \delta_0, \\ \dot{q}_{0,\text{mb}} = D_{\text{obm}} z_0. \end{gathered} \tag{38}$$

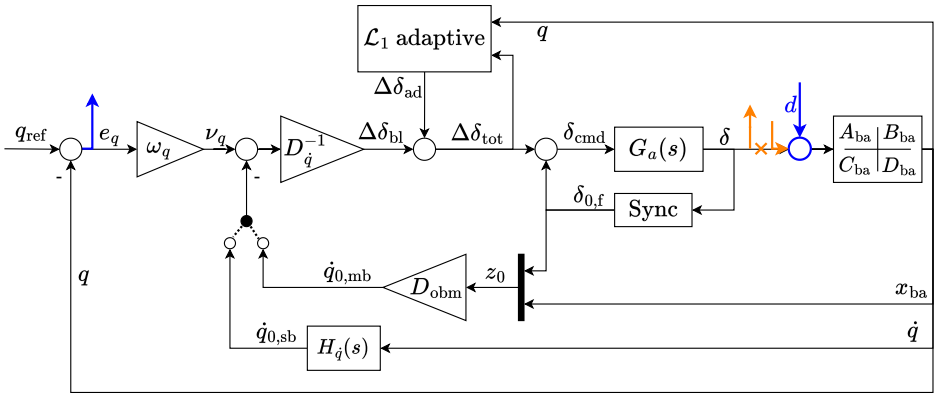

Fig. 7 Transfer function analysis points in the linearized closed loop system.

for the model-based INDI and by

$$\Delta\delta_{\text{cmd,sb}} = D_{\dot{q}}^{-1}(\nu_q - \dot{q}_{0,sb}), \quad \delta_{\text{cmd}} = \Delta\delta_{\text{cmd,sb}} + \delta_{0,\text{f}}, \quad \delta_{0,\text{f}}(s) = H_{\dot{q}}(s)\delta_0.$$
$$\dot{q}_{0,\text{sb}}(s) = H_{\dot{q}}(s)\dot{q}_0(s), \tag{39}$$

for the sensor-based INDI. The IDI controllers, the $\mathcal{L}_1$ adaptive controller and the outer loops of the autopilot are implemented in a separate Simulink® model, where the `linearize` function is used to extract relevant transfer functions. In the next section the just-described methodology is used to evaluate the influence of the tuning of the adaptive controller on the performance and robustness of the closed loop system featuring model-based and sensor-based INDI architectures.

5.2 Sensitivity to the adaptive controller tuning parameters

In the following frequency domain analysis, we construct linear approximations of the closed loop and focus on two relevant properties: disturbance rejection capabilities within the inner pitch rate control loop, and the stability robustness of the closed-loop system. In particular, the sensitivity to the tuning of the parameters in the $\mathcal{L}_1$ PwC adaptive controller is analyzed separately when considering the baseline model-based INDI controller and the sensor-based one, presented in Sections 4.2.1 and 4.2.2. For all of the analyses which follow, the bare airframe is trimmed at $V = 1000\,\text{m/s}$, $h = 5000\,\text{m}$. The tuning of the sensor-based and model-based baseline INDI controllers and of the outer-loops controllers is unchanged from those defined in Table 1, and a sweep of the filter bandwidth ω_{f} and of the predictor stabilizing gain L of the $\mathcal{L}_1$ PwC adaptive controller is considered.

5.2.1 Disturbance rejection performance analysis

We first look at the disturbance rejection properties of the inner pitch rate control loop, which is the focus of the adaptive augmentation. With reference to Fig. 7, it is desirable that the magnitude of the closed-loop transfer function from the disturbance d injected at the plant input to the tracking error $e_q \coloneqq q_{\text{ref}} - q$ is small in the low-frequency range, where the effect of slowly-varying disturbances can mitigated through the action of feedback. To isolate the behavior of the INDI and $\mathcal{L}_1$ adaptive controllers, the outer controllers of the autopilot are disconnected via a loop break.

Fig. 8 shows the results obtained for the baseline sensor-based INDI controller. Note that in each of the sub-figures, the $\mathcal{L}_1$ filter bandwidth is fixed to a different value while the predictor stabilizing gain is varied. As expected, the baseline sensor-based INDI as a standalone features an inherent integral action in the control law, just like it was anticipated in Section 2.2 and observed in many works. The $\mathcal{L}_1$ PwC adaptive augmentation acts primarily at low-frequencies, where it reduces the magnitude of the transfer function, thereby improving the disturbance rejection capabilities. The peak magnitude of the transfer

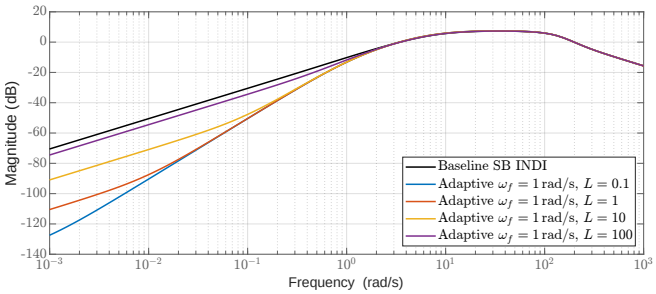

(a) Sensor-based INDI with $\mathcal{L}_1$ with $\omega_\mathrm{f} = 1$ rad/s and varying L.

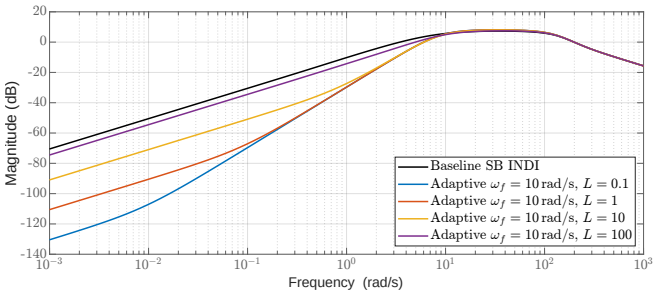

(b) Sensor-based INDI with $\mathcal{L}_1$ with $\omega_\mathrm{f} = 10$ rad/s and varying L.

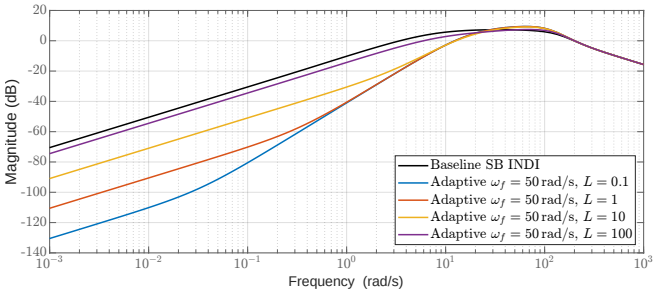

(c) Sensor-based INDI with $\mathcal{L}_1$ with $\omega_\mathrm{f} = 50$ rad/s and varying L.

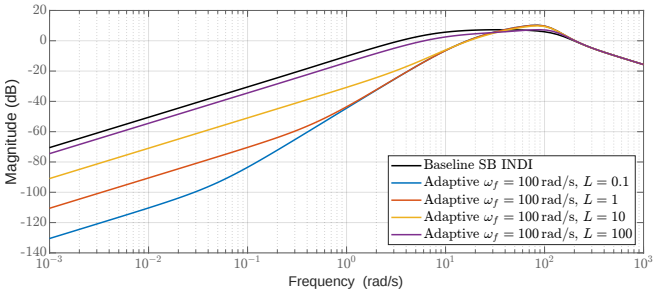

(d) Sensor-based INDI with $\mathcal{L}_1$ with $\omega_\mathrm{f} = 100$ rad/s and varying L.

Fig. 8 Closed-loop disturbance rejection for the sensor-based baseline INDI and varying adaptive controller parameters ω_f, L.

functions increases for combinations of large ω_f and small L, which can be connected to the overshooting pitch rate response observed in Fig. 6, and to the tuning remarks for the $\mathcal{L}_1$ controller outlined in Section 3.3.

The results arising from the same analysis performed on a baseline model-based INDI controller are displayed in Fig. 9. As expected, the model-based architecture with a simple proportional pseudo-control law does not present the inherent integral contribution which is characteristic of the sensor-based architecture. Therefore, the considered model-based INDI does not mitigate the effect of slowly-varying disturbances. This explains why it is advised to include an integral action in the pseudo control law when adopting a model-based design, similarly to a standard NDI [30]. In this case, the $\mathcal{L}_1$ PwC adaptive controller greatly improves the mitigation of low-frequency disturbances by reducing the steady state gain of the closed loop transfer function.

In both architectures it is observed that large values of the $\mathcal{L}_1$ filter bandwidth extend the frequency range in which disturbances are mitigated, while small values for the predictor stabilizing gain mainly decrease the magnitude of the transfer function at low frequencies, corresponding to a better estimation of the disturbance, like it was explained analitically in Section 3.3.

5.2.2 Robustness analysis with Nyquist criterion

Despite the performance analysis clearly indicates that the $\mathcal{L}_1$ adaptive augmentation is beneficial to both baseline architectures (albeit to different scales), the stability of the system must be also investigated. To do this, the loop-transfer function at the plant input is computed as shown in Fig. 7, and the Nyquist stability criterion is applied. In particular, Nichols charts are used to visualize the magnitude and phase of the loop-transfer function frequency response in comparison to the critical point, corresponding to unit magnitude and -180 deg phase shift.

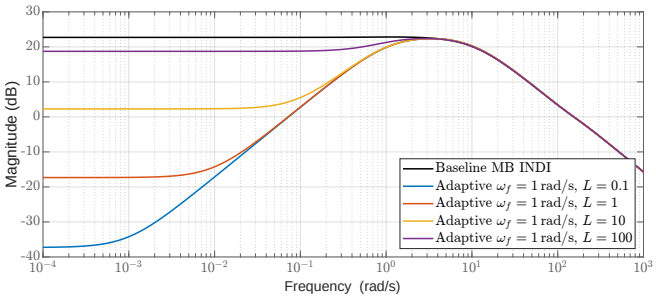

(a) Model-based INDI with $\mathcal{L}_1$ with $\omega_\mathrm{f} = 1$ rad/s and varying L.

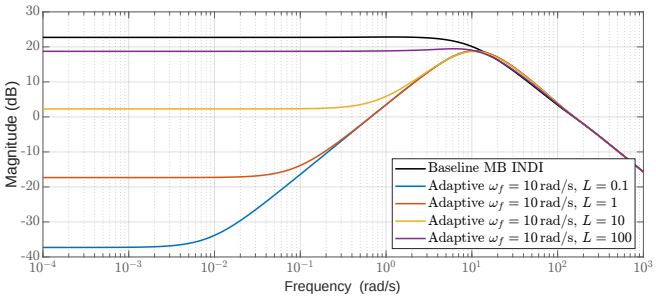

(b) Model-based INDI with $\mathcal{L}_1$ with $\omega_\mathrm{f} = 10$ rad/s and varying L.

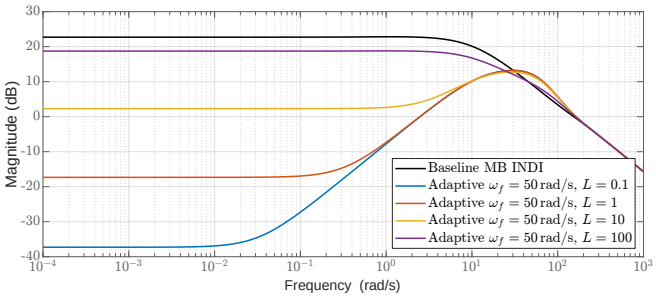

(c) Model-based INDI with $\mathcal{L}_1$ with $\omega_\mathrm{f} = 50$ rad/s and varying L.

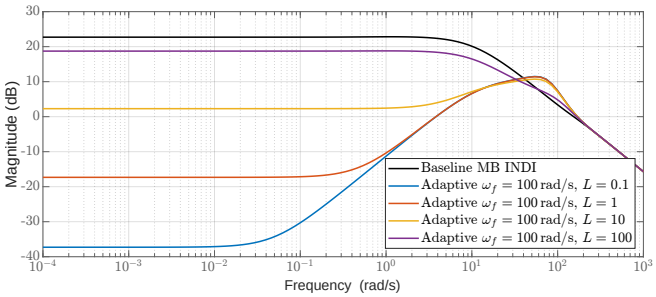

(d) Model-based INDI with $\mathcal{L}_1$ with $\omega_\mathrm{f} = 100$ rad/s and varying L.

Fig. 9 Closed-loop disturbance rejection for the model-based baseline INDI and varying adaptive controller parameters ω_f, L.

Fig. 10 shows the results obtained using the baseline sensor-based INDI controller. In this case, the $\mathcal{L}_1$ adaptive augmentation tends to reduce the stability margins of the system (and therefore the robustness to gain a phase shifts) when compared to the standalone baseline controller. Large values of the filter bandwidth coupled with small values of stabilizing gain tend to reduce the gain and phase margins. As expected, for the opposite case the frequency responses of the loop-transfer functions tend to that of the baseline INDI controller.

The same analysis is performed on the model-based baseline controller, with the results shown in Fig. 11. For this architecture, the tuning of the adaptive controller does not necessarily reduce the stability margins. In fact, for some combination of values of the filter bandwidth and the stabilizing gain, the margins of the closed-loop system are actually increased, as visible in some of the curves in Fig. 11(c). This can be traced back to the fact for the model-based architecture the proportional pseudo-control law does not yield any integral action in the loop transfer function, and with a correctly tuned $\mathcal{L}_1$ adaptive controller the designer may increase the magnitude of the loop transfer at low frequencies, effectively giving very significant improvements to both stability and low-frequency disturbance rejection.

The stability analysis shows that the controller parameters adopted in Section 4 and shown in Table 1 achieve acceptable gain and phase margins, shown in Tab. 2 and Tab. 3, for both INDI architectures. It is important to note that with respect to the sensor-based baseline, the augmentation reduces the margins, while the opposite happens for the model-based baseline INDI controller. Another important observation is that autopilot with an inner loop sensor-based INDI controller shows a higher crossover frequency than the model-based version, and that for both baseline controllers the $\mathcal{L}_1$ adaptive augmentation increases the gain-crossover frequency.

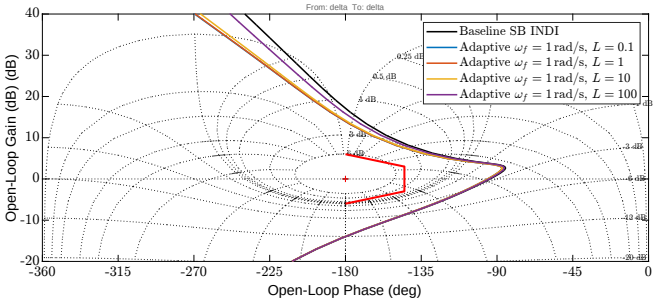

(a) Sensor-based INDI and $\mathcal{L}_1$ filter bandwidth $\omega_\mathrm{f} = 1\,\mathrm{rad/s}$.

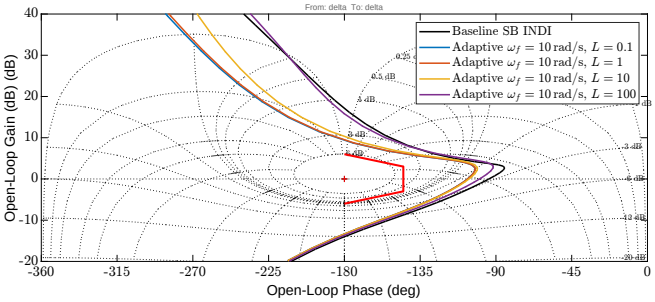

(b) Sensor-based INDI and $\mathcal{L}_1$ filter bandwidth $\omega_\mathrm{f} = 10\,\mathrm{rad/s}$.

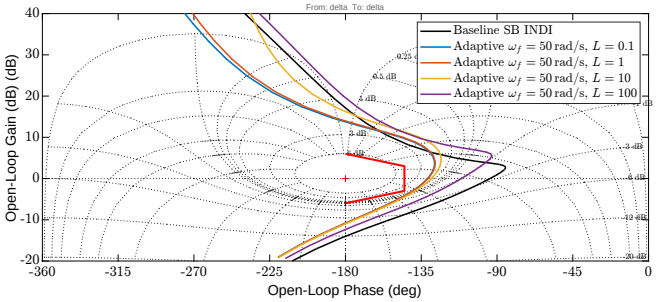

(c) Sensor-based INDI and $\mathcal{L}_1$ filter bandwidth $\omega_\mathrm{f} = 50\,\mathrm{rad/s}$.

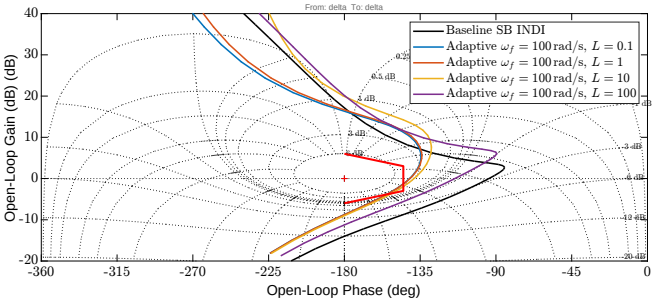

(d) Sensor-based INDI and $\mathcal{L}_1$ filter bandwidth $\omega_\mathrm{f} = 100\,\mathrm{rad/s}$.

Fig. 10 Loop-transfer function analysis for the sensor-based baseline INDI and varying adaptive controller parameters ω_f, L.

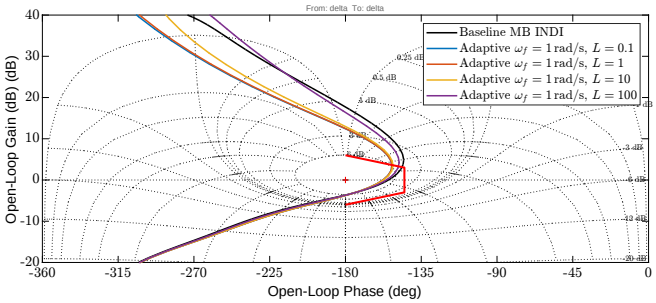

(a) Model-based INDI with $\mathcal{L}_1$ filter bandwidth $\omega_\mathrm{f} = 1\,\mathrm{rad/s}$.

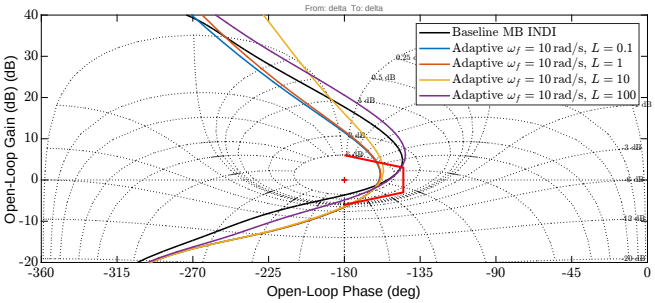

(b) Model-based INDI with $\mathcal{L}_1$ filter bandwidth $\omega_\mathrm{f} = 10\,\mathrm{rad/s}$.

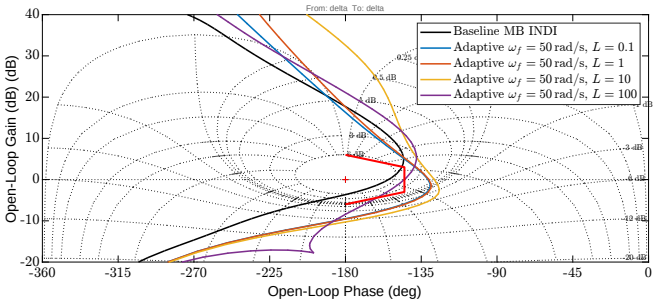

(c) Model-based INDI with $\mathcal{L}_1$ filter bandwidth $\omega_\mathrm{f} = 50\,\mathrm{rad/s}$.

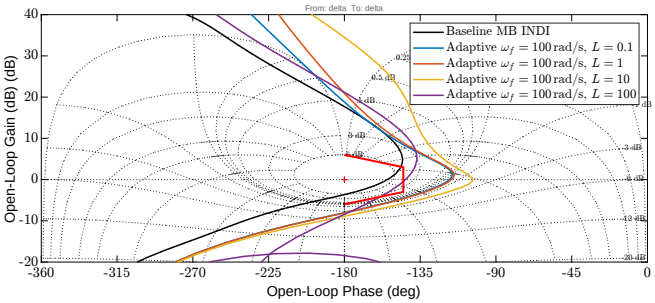

(d) Model-based INDI with $\mathcal{L}_1$ filter bandwidth $\omega_\mathrm{f} = 100\,\mathrm{rad/s}$.

Fig. 11 Loop-transfer function analysis for the model-based baseline INDI and varying adaptive controller parameters ω_f, L.

Table 2 Gain margins GM and and phase margins PM of the sensor-based autopilot tuning from Table 1.

	GM (dB)	PM (deg)
Standalone Baseline SB INDI	14.0 @(179.5 rad/s)	85.9 @(39.1 rad/s)
Adaptive $\omega_f = 50\,\mathrm{rad/s}$, $L = 1$	10.8 @(156.8 rad/s)	49.0 @(55.8 rad/s)

Table 3 Gain margins GM and and phase margins PM of the model-based autopilot tuning from Table 1.

	GM (dB)	PM (deg)
Standalone Baseline MB INDI	3.7 @(11.7 rad/s)	25.6 @(5.8 rad/s)
Adaptive $\omega_f = 50\,\mathrm{rad/s}$, $L = 1$	9.6 @(68.4 rad/s)	49.5 @(16.1 rad/s)

6 Conclusions

In the presented work, frequency-domain analysis methods were used to add insights into the stability and robustness properties of $\mathcal{L}_1$-augmented INDI controllers. The application scenario of a longitudinal autopilot played a crucial role in verifying known tuning trade-offs in the two controllers, and in providing new insights on the potentialities of the proposed control architecture. The $\mathcal{L}_1$ PwC adaptive augmentation proves to be very beneficial to the model-based baseline INDI controller, as both the disturbance rejection capabilities and the stability margins can be increased with a correct tuning. With the sensor-based INDI, the mitigation of disturbances is improved, although it is less marked given the integral contribution already present in the baseline controller, while the stability margins are reduced, showing that an important performance-robustness trade-off exists. It is recognized that the obtained results are not of general nature, as a single-input plant was considered. Nevertheless, the adopted methodology for the frequency-domain analysis can be easily generalized to increase the potentialities of the work, where the aim could be to perform an optimal one-step tuning of the two controllers, explicitly incorporating performance and robustness requirements, and analyzing robustness through more general tools such as the structured singular value.

Declaration of Use of Artificial Intelligence

Artificial intelligence was used in the work presented for proofreading.

References

[1] Pascal Gahinet and Pierre Apkarian. Automated tuning of gain-scheduled control systems. In *Proceeding of the 52nd IEEE Conference on Decision and Control*, pages 2740–2745, 2013. doi: 10.1109/CDC.2013.6760297.

[2] R. C. van't Veld. Incremental nonlinear dynamic inversion flight control. Master's thesis, Delft university of Technology, 2016.

[3] P Smith. A simplified approach to nonlinear dynamic inversion based flight control. In *23rd atmospheric flight mechanics conference*, page 4461, 1998.

[4] Jeffrey J Harris. F-35 flight control law design, development and verification. In *2018 Aviation Technology, Integration, and Operations Conference*, page 3516, 2018.

[5] S Sieberling, QP Chu, and JA Mulder. Robust flight control using incremental nonlinear dynamic inversion and angular acceleration prediction. *Journal of guidance, control, and dynamics*, 33(6):1732–1742, 2010.

[6] Xuerui Wang, Erik-Jan Van Kampen, Qiping Chu, and Peng Lu. Stability analysis for incremental nonlinear dynamic inversion control. *Journal of Guidance, Control, and Dynamics*, 42(5):1116–1129, 2019.

[7] Ewoud J. J. Smeur, Qiping Chu, and Guido C. H. E. De Croon. Adaptive incremental nonlinear dynamic inversion for attitude control of micro air vehicles. *Journal of Guidance, Control, and Dynamics*, 39(3):450–461, 2016.

[8] Tijmen Pollack and Erik-Jan Van Kampen. Robust stability and performance analysis of incremental dynamic-inversion-based flight control laws. *Journal of Guidance, Control, and Dynamics*, 46(9):1785–1798, 2023.

[9] Yagiz Kumtepe, Tijmen Pollack, and Erik-Jan Van Kampen. Flight control law design using hybrid incremental nonlinear dynamic inversion. In *Proceedings of the AIAA SCITECH Forum*. American Institute of Aeronautics and Astronautics, 2022. doi: 10.2514/6.2022-1597.

[10] Leonardo S Encarnação, Tijmen Pollack, Gertjan Looye, and Spilios Theodoulis. Multi-objective synthesis of hybrid incremental dynamic inversion control laws using h-infinity loop-shaping. In *AIAA SCITECH 2026 Forum*, page 0551, 2026.

[11] Jiannan Zhang, Jian Wang, Fubiao Zhang, and Florian Holzapfel. Modeling and incremental nonlinear dynamic inversion control for a highly redundant flight system. In *AIAA Scitech 2019 Forum*, page 1922, 2019.

[12] Agnes Steinert, RAAB Stefan, Simon Hafner, Florian Holzapfel, and HONG Haichao. From fundamentals to applications of incremental nonlinear dynamic inversion: A survey on INDI – Part I. *Chinese Journal of Aeronautics*, page 103553, 2025.

[13] S. Sieberling, Q. P. Chu, and J. A. Mulder. Robust Flight Control Using Incremental Nonlinear Dynamic Inversion and Angular Acceleration Prediction. *Journal of Guidance, Control, and Dynamics*, 33:1732–1742, Nov. 2010. doi: 10.2514/1.49978.

[14] Chengyu Cao and Naira Hovakimyan. Design and analysis of a novel L1 adaptive control architecture with guaranteed transient performance. *IEEE Transactions on Automatic Control*, 53(2):586–591, 2008.

[15] Naira Hovakimyan and Chengyu Cao. $\mathcal{L}_1$ *adaptive control theory: guaranteed robustness with fast adaptation*. SIAM, 2010.

[16] Evgeny Kharisov, Naira Hovakimyan, and Karl Åström. Comparison of several adaptive controllers according to their robustness metrics. In *Proceedings of the AIAA Guidance, Navigation, and Control Conference*. American Institute of Aeronautics and Astronautics, 2010. doi: 10.2514/6.2010-8047.

[17] Chen Qi and Ai Jianliang. NDI-based $\mathcal{L}_1$ adaptive control design for a generic hypersonic vehicle model. In *Proceedings of the AIAA Guidance, Navigation, and Control Conference*. American Institute of Aeronautics and Astronautics, 2017. doi: 10.2514/6.2017-1248.

[18] Steven Snyder, Pan Zhao, and Naira Hovakimyan. $\mathcal{L}_1$ adaptive control with switched reference models: application to learn-to-fly. *arXive*, pages 1–34, 2022.

[19] Tyler Leman, Enric Xargay, Geir Dullerud, Naira Hovakimyan, and Thomas Wendel. L1 adaptive control augmentation system for the x-48b aircraft. In *AIAA guidance, navigation, and control conference*, page 5619, 2009.

[20] Christopher M Elliott, Joshua A Harris, and Greg Tallant. L1 adaptation as a bolt-on robustifying control law to a baseline dynamic inversion system. In *2018 IEEE Aerospace Conference*, pages 1–8. IEEE, 2018.

[21] Brian L. Stevens, Frank L. Lewis, and Eric N. Johnson. *Aircraft control and simulation: dynamics, controls design, and autonomous systems*. John Wiley & Sons, 2016.

[22] Eric N Johnson and Anthony J Calise. Pseudo-control hedging: a new method for adaptive control. In *Proceedings of the Advances in navigation guidance and control technology workshop*, pages 1–2. Alabama, USA, 2000.

[23] Pranav Bhardwaj, Venkata Sravan Akkinapalli, Jiannan Zhang, Saurabh Saboo, and Florian Holzapfel. Adaptive augmentation of incremental nonlinear dynamic inversion controller for an extended F-16 model. In *Proceedings of the AIAA Scitech Forum*. American Institute of Aeronautics and Astronautics, 2019. doi: 10.2514/6.2019-1923.

[24] Sofiane Pineau, Spilios Theodoulis, Michel Zasadzinski, Mohamed Boutayeb, and Emmanuel Roussel. L1 adaptive augmentation of an incremental nonlinear dynamic inversion autopilot for dual-spin guided projectiles. In *AIAA SCITECH 2023 Forum*, page 1998, 2023.

[25] Naira Hovakimyan, Chengyu Cao, Evgeny Kharisov, Enric Xargay, and Irene M. Gregory. $\mathcal{L}_1$ adaptive control for safety-critical systems. *IEEE Control Systems*, 31:54–104, 2011. doi: 10.1109/MCS.2011.941961.

[26] Thomas Bierling. *Comparative analysis of adaptive control techniques for improved robust performance*. PhD thesis, Technische Universität München, 2014.

[27] Anders Pettersson, Karl J Åström, Anders Robertsson, and Rolf Johansson. Analysis of linear l1 adaptive control architectures for aerospace applications. In *2012 IEEE 51st IEEE conference on decision and control (CDC)*, pages 1136–1141. IEEE, 2012.

[28] Mathworks®. Tuning of gain-scheduled three-loop autopilot, 2013. `https://it.mathworks.com/help/control/ug/tuning-of-gain-scheduled-three-loop-autopilot.html`.

[29] Giorgio Raos. Enhancing incremental NDI control with $\mathcal{L}_1$ adaptive augmentation in a longitudinal autopilot. Master's thesis, Politecnico di Milano, Milan, Italy, 2024.

[30] Rick Hyde and George Papageorgiou. Analysing the stability of ndi-based flight controllers with lpv methods. In *AIAA Guidance, Navigation, and Control Conference and Exhibit*, page 4039, 2001.